

# STARS

University of Central Florida  
**STARS**

---

Honors Undergraduate Theses


UCF Theses and Dissertations

---

2018

## Investigating the Role of the Caspase-6 Cleavage Fragment of Mutant Huntingtin in Huntington Disease Pathogenesis

Jourdan A. McKinnis  
*University of Central Florida*

 Part of the [Other Neuroscience and Neurobiology Commons](#)  
Find similar works at: <https://stars.library.ucf.edu/honorsthesis>  
University of Central Florida Libraries <http://library.ucf.edu>

This Open Access is brought to you for free and open access by the UCF Theses and Dissertations at STARS. It has been accepted for inclusion in Honors Undergraduate Theses by an authorized administrator of STARS. For more information, please contact [STARS@ucf.edu](mailto:STARS@ucf.edu).

---

### Recommended Citation

McKinnis, Jourdan A., "Investigating the Role of the Caspase-6 Cleavage Fragment of Mutant Huntingtin in Huntington Disease Pathogenesis" (2018). *Honors Undergraduate Theses*. 395.  
<https://stars.library.ucf.edu/honorsthesis/395>



INVESTIGATING THE ROLE OF THE CASPASE-6 CLEAVAGE FRAGMENT OF  
MUTANT HUNTINGTIN IN HUNTINGTON DISEASE PATHOGENESIS

by

JOURDAN A. MCKINNIS

A thesis submitted in partial fulfillment of the requirements  
for the Honors in the Major Program in Biomedical Sciences  
in the College of Medicine  
and in the Burnett Honors College  
at the University of Central Florida  
Orlando, Florida

Spring Term, 2018

Thesis Chair: Amber Southwell, Ph.D.

© 2018 Jourdan Mckinnis

## ABSTRACT

Huntington disease (HD) is a devastating and fatal neurodegenerative disease. At the moment, no disease modifying therapies are available, with only symptomatic treatment offered to alleviate psychiatric and some types of motor deficits. As a result, many people will continue to suffer and die from this disease. Small molecule therapies have failed to provide benefit in HD, necessitating more complex gene therapy approaches and the identification of less traditional therapeutic targets. A previous study demonstrated that preventing cleavage of the huntingtin (HTT) protein, the protein that when mutated causes HD, by caspase 6 (C6) at amino acid 586 prevents the onset of disease in transgenic HD model mice. This suggests that inhibiting the toxicity initiated by N586 cleavage could be a promising therapeutic strategy, but a safe and specific way to do this in humans has not been identified. General C6 inhibition is not a feasible strategy due to the vital functions it plays throughout life. Thus, the purpose of this study was to investigate whether the C6 cleavage fragment of HTT, N586, is itself a toxic species of HTT or if it initiates a toxic proteolytic pathway in order to identify more viable therapeutic strategies for HD. To accomplish this, we are using novel and highly sensitive immunoprecipitation and flow cytometry (IP-FCM) protein detection assays, specific for the N586 neopeptide of HTT, to evaluate the *in vivo* persistence of N586 in HD model mice. If N586 is detected, it is likely that it is itself toxic and promoting its degradation may be beneficial. Conversely, if it is not detected, N586 cleavage likely initiates a toxic degradation pathway and promoting its stability may be beneficial.

The results of these studies have the potential to define new therapeutic strategies for HD that can be addressed more specifically than generalized C6 inhibition for the prevention of N586-mediated toxicity. The selective targeting of N586 toxicity, either to promote or prevent its degradation depending on our results, would ensure that therapeutic activity is restricted to HTT and reduce the potential for deleterious off-target effects

## **DEDICATION**

To my mentor, Dr. Amber Southwell, for taking a chance on me

and

To my parents for always believing in my dreams and encouraging me every step of the way.

## ACKNOWLEDGMENTS

I would like to thank the UCF Office of Undergraduate Research for generously supporting my research through the Summer Undergraduate Research Fellowship program and awarding me with a grant to help fund my project. I thank Michael Hayden and Nicholas Caron at the University of British Columbia in Vancouver for generously donating the N586 constructs and neo-epitope-specific antibodies, along with Hailey Findlay-Black and Stephen Smith for sharing their protocols with me and consulting on optimization. I would also like to thank my committee members, Dr. Sugaya and Dr. Hashim, for seeing me through this journey.

Special thanks to the members of the Southwell lab for their continuous encouragement, and specifically Dr. Yaunyun Xie, for his expertise and always being there to assist me during my experiments. Last but not least, I thank my incredible mentor, Dr. Amber Southwell, for her never ending patience and support throughout the entirety of this project. None of this would have been possible without her.

## TABLE OF CONTENTS

LIST OF FIGURES .....	viii
LIST OF TABLES .....	ix
LIST OF ABBREVIATIONS.....	x
CHAPTER I. INTRODUCTION.....	1
CHAPTER II. RESULTS .....	8
IVLD/HD55 and IVLD/MW1 are the Highest Affinity N586 IP-FCM Antibody Pairs .....	8
Purifying N586 From Brain Lysate Digested With C6 Enzyme .....	12
Purification of Recombinant N586 Protein From Bacterial Expression.....	15
CHAPTER III. DISCUSSION.....	20
CHAPTER IV. METHODOLOGY .....	24
Primary Antibodies .....	24
Hu97/18 Brain Microdissection.....	24
Covalent-Coupling of IVLD to CML Beads .....	25
Purification of N586 Protein from Brain lysate .....	25
Western Blotting .....	27
IP-FCM of Brain Lysate .....	27
Generation of Recombinant N586 Protein.....	29
Purification of MBP-tagged Proteins.....	29
REFERENCES .....	31



## LIST OF FIGURES

Figure 1. Schematic of detection of mHTT in CSF by immunoprecipitation and flow cytometry	5
Figure 2. Demonstration of IP-FCM sensitivity and specificity.....	6
Figure 3. The neo-htt586 antibody specifically detects huntingtin 586 amino acid fragments....	10
Figure 4. Screen for N586 IP-FCM capture/probe antibody pairs.....	11
Figure 5. C6 cut N586 protein Western blot.....	13
Figure 6. N586 IP-FCM results with IVLD/MW1 and IVLD/HD55. ....	14
Figure 7. Restriction enzyme digestion. ....	16
Figure 8. Ponceau stain of N586.....	18
Figure 9. Recombinant N586 protein Western blot.....	19

## **LIST OF TABLES**

Table 1. Purified N586-Q15 and Q68 MBP fusion protein elution fraction A280 readings ..... 17

## LIST OF ABBREVIATIONS

Ab = Antibody

ACSF = Artificial cerebrospinal fluid

ATP = Adenosine triphosphate

BSA = Bovine serum albumin

C6 = Caspase-6

C6R = Caspase-6 resistant

cAMP = Cyclic adenosine monophosphate

cGMP = Cyclic guanine monophosphate

CHAPs = 3-((3-cholamidopropyl) dimethylammonio)-1-propanesulfonate

CML = Carboxylate-modified polystyrene latex

CNS = Central Nervous System

CoQ10 = Coenzyme Q10

CSF = Cerebrospinal fluid

ddH<sub>2</sub>O = Double-distilled deionized water

DHSB = Developmental Studies Hybridoma Bank

DTT = Dithiothreitol

EDAC = 1-Ethyl-3-(3-Dimethylaminopropyl)carbodiimide, Hydrochloride

EDTA = Ethylenediaminetetraacetic acid

HD = Huntington Disease

HTT = Huntingtin

IP-FCM = Immunoprecipitation followed by flow-cytometry

LDS = Lithium dodecyl sulfate

MBP = Maltose binding protein

MES = 2-(N-Morpholino)ethanesulfonic acid

MFI = Median fluorescence intensity

mt = Mutant

mtHTT = Mutant huntingtin

NaCl = Sodium chloride

NaF = Sodium Fluoride

NaN<sub>3</sub> = Sodium azide

NMDAR = N-Methyl-D-aspartate

NP40 = Nonidet P40

OD = Optical density

PBS = Phosphate buffered saline

SDS-PAGE = Sodium dodecyl sulfate polyacrylamide gel

TBE = Tris/Borate/EDTA

wt = Wild-type

YAC = Yeast Artificial Chromosome

## CHAPTER I. INTRODUCTION

Huntington Disease (HD) is an autosomal dominant neurodegenerative disease caused by a mutation in the short arm of chromosome 4 that codes for an expanded CAG repeat in exon 1 of the huntingtin (*HTT*) gene<sup>1</sup>. Normal individuals can have CAG repeat sizes anywhere from 9-24, whereas individuals with HD will have CAG repeats greater than 35, with reduced penetrance from 36 to 39<sup>2</sup>. Furthermore, juvenile onset occurs in individuals with repeats greater than 60<sup>3</sup>. This expanded CAG repeat results in the translation of an abnormally long mutant HTT (mHTT) protein that interferes with many cellular pathways, resulting in cell degeneration and death. The brain regions most affected in HD are the basal ganglia<sup>4</sup>, including the caudate nucleus and the putamen, which are largely responsible for voluntary motor control, in addition to motor learning, executive functions, behavior, and emotions<sup>5</sup>. Other areas of degeneration include the cortex<sup>6,7</sup> and white matter<sup>8</sup>.

Individuals with HD exhibit motor dysfunction such as loss of fine motor control, motor impersistence, gait abnormalities, and uncontrollable movements known as chorea, as well as cognitive and psychiatric deficits including memory loss, anxiety, and depression<sup>9</sup>. HD is incurable and fatal, resulting in death typically 15-20 years after onset<sup>10</sup>, and is extremely debilitating for patients and their loved ones. At the moment, there are no disease-modifying treatments for HD, only moderately beneficial symptomatic treatments, such as antidepressants for depression and tetrabenazine for chorea<sup>11</sup>.

Traditional small molecule approaches to the treatment of HD have failed, likely due to the complexity of the protein and the disease pathogenesis. HD is a multifaceted disease in which

many molecules and cellular processes are perturbed. The reason being that HTT is an incredibly large and promiscuous protein playing a role in multiple cellular pathways and having many binding partners within the cell. Major functions of HTT include transcriptional regulation, regulation of energy production, vesicle transport, protein homeostasis, synaptic function, stress response signaling, scaffolding, autophagosome cargo recognition, and NMDAR regulation<sup>12,13</sup>. It has many binding partners, including proteins, nucleic acids, and organelles<sup>13,14</sup>. The promiscuity and diverse functions of HTT and the resulting wide range of cellular processes perturbed by mtHTT are likely the reason that traditional small molecule therapeutic approaches, which typically target a single pathologic process, have failed.

For instance, the largest ever study in HD patients sought to improve mitochondrial function and reduce oxidative stress by coenzyme Q10 (CoQ10) treatment. CoQ10 is an enzyme that plays a role in oxidative phosphorylation and acts as an antioxidant, but the trial was halted early for futility<sup>15</sup>. Other failed therapeutic approaches targeting single molecules and pathways include the CREST-E study, which focused on improving impaired energy production by providing creatinine supplements<sup>16</sup>, a high energy phosphate source for restoring adenosine triphosphate (ATP), and the Amaryllis trial, which focused on facilitating neuronal communication and signaling through inhibition of phosphodiesterase-10<sup>17</sup>, a regulator for both cAMP and cGMP signaling cascades<sup>18</sup>. The failure of these therapeutic approaches is likely due to targeting single pathologic processes, when in reality there are so many processes and pathways affected by HD that treating one or a few is ineffective, leaving a multitude unchanged. Thus, therapeutic approaches that modulate mtHTT, the direct cause of the disease, have a greater likelihood of success.

A previous study demonstrated that preventing cleavage at the amino acid 586 caspase-6 (C6) cleavage site of HTT prevents the onset of disease in a transgenic mouse model of HD, YAC128. YAC128 mice carry a full-length human *mtHTT* transgene and display a wide variety of HD-like characteristics such as anxiety and depressive-like behavior, cognitive deficits, and progressive motor deficits. Additionally, these mice undergo selective striatal neurodegeneration<sup>19,20</sup>. A companion line, C6R, was created with a mutation in the C6 cleavage site located in exon 13; thus, expressing an identical *mtHTT* transgene that cannot be cleaved by C6. C6R mice express similar amounts of *mtHTT* as YAC128 mice and display widespread HTT aggregation in the brain. However, C6R mice are completely protected from *mtHTT* toxicity, and do not display any of the HD-like behavioral or neuropathological changes observed in YAC128 mice, indicating protection from disease. These data suggest that N586 cleavage of HTT is a rate-limiting step in HD pathogenesis and that inhibiting the subsequent toxicity may be a promising therapeutic strategy for HD.

Inhibiting N586-linked toxicity by systemic inhibition of C6 is a non-specific and potentially deleterious strategy considering that C6 activity has vital function throughout life. For instance, in adults the region with highest C6 expression is the colon, where it likely plays a critical role in ongoing apoptosis. Supporting this is the finding that the active form of C6 is reduced in colon cancer<sup>21</sup>. Thus, systemic C6 inhibition may promote colon cancer. Therefore, a more specific therapeutic strategy, addressing only the HTT N586 cleavage event, would be preferable. HTT is processed through a variety of proteolytic events and pathways<sup>22</sup>, and N-terminal cleavage fragments of *mtHTT* likely play a predominant role in HD pathogenesis. Supporting this is the earlier onset and greater severity of HD-like signs in transgenic mouse

models of HD expressing an N-terminal mtHTT fragment as compared to full-length mtHTT models<sup>23</sup>. Thus, by investigating the location and quantity of N586 in the brains of HD mice and in their biofluids, we hope to infer a possible role of N586 in HD pathogenesis, whether it be the direct toxicity of the fragment itself or the toxicity of its degradation pathway.

Because N586 is only 1 of many species of mtHTT, a highly sensitive method would likely be required to quantify it, even in brain tissue, where HTT protein is abundant<sup>24</sup>. Immunoprecipitation and flow cytometry (IP-FCM) is a highly sensitive method of protein detection that our lab has adapted to quantify mtHTT in HD patient and mouse cerebrospinal fluid (CSF)<sup>25,26</sup>, where HTT protein is extremely low abundance (Figure 1). IP-FCM is highly sensitive at detecting extremely low mtHTT concentrations in biofluids with up to femtomolar detection (Figure 2). In order to develop an N586-specific IP-FCM assay to investigate the *in vivo* persistence of N586, our lab screened anti-HTT antibody combinations including one or both of a pair of N586 neoepitope-specific antibodies previously generated by Michael Hayden's laboratory at the University of British Columbia<sup>27</sup>.



## Immunoprecipitation and flow cytometry (IP-FCM) mHTT detection

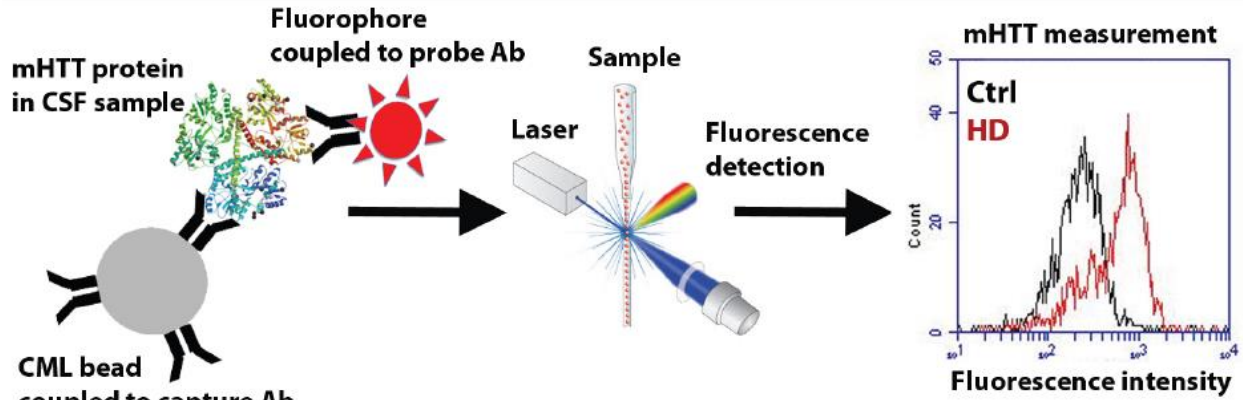


**Figure 1. Schematic of detection of mHTT in CSF by immunoprecipitation and flow**

**cytometry**<sup>28</sup> CML latex beads coupled to capture antibody were bound to mHTT in the CSF of HD patients or controls. Fluorophore conjugated probe Ab was then bound to the protein. Relative concentration of mHTT was measured using a flow cytometer to measure the fluorescence intensity of the beads. Bead count vs fluorescence intensity is shown with the control CSF in black and the HD CSF in red.

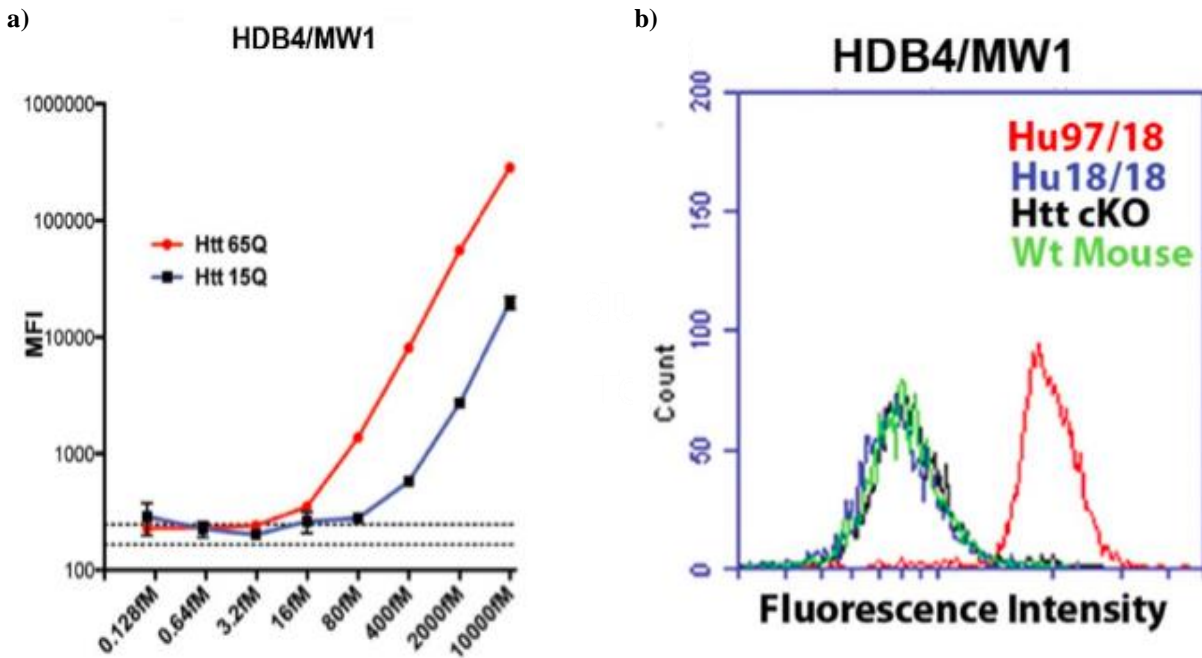


**Figure 2. Demonstration of IP-FCM sensitivity and specificity.** “(A) HTT-IP-FCM median fluorescence intensity (MFI) using serial dilutions of recombinant HTT fusion protein with 15 or 65 Q in ACSF using HDB4/MW1. Dashed lines indicate the mean  $\pm$  SEM of the no-protein controls, showing assay background. (B) HTT IP-FCM in brain lysates from Hu97/18, Hu18/18, conditional Htt KO, and wildtype mice using HDB4/MW1.”<sup>25</sup> Taken together these results indicate that IP-FCM is extremely sensitive up to 16 fM, as well as, specific in that it can detect mtHTT from wt.

In this study, we set out to characterize the specificity and sensitivity of the high affinity antibody pairs identified in this screen for use in the detection of N586 in brain tissue and biofluids of HD model mice with the goal of eventually using them to investigate the location and quantity of N586 in HD mouse brain and biofluids. If we find that N586 persists in brain tissue, it may be an indicator of its direct toxicity. Thus, as a therapeutic approach, it might be desirable to promote degradation of the fragment. Alternatively, if N586 is not detected, this may indicate that the cleavage event initiates a toxic proteolytic pathway. In which case, a possible therapeutic strategy may be to stabilize N586. The results of this study could identify novel therapeutic targets and strategies for the treatment of HD.

## CHAPTER II. RESULTS

### **IVLD/HD55 and IVLD/MW1 are the Highest Affinity N586 IP-FCM Antibody Pairs**

Our lab previously conducted a screen for IP-FCM capture/probe pairs with high affinity for N586. Six anti-HTT antibodies (Abs) were used in the screen; 2 specific for the N586 neoepitope (HD55 and IVLD)<sup>27</sup> (Figure 3) and 4 specific for additional target sites i.e. the N-terminus (BKP1)<sup>29</sup>, an epitope near the C-terminus of N586 (2166)<sup>30</sup>, polyproline (MW7)<sup>31</sup>, and expanded polyglutamine, (MW1)<sup>31</sup>. Only combinations including at least one of the N586 neoepitope antibodies were screened, resulting in 18 combinations (Figure 4). To determine total amount of N586, we wanted Ab combinations to recognize both mt and wtN586, so combinations were screened against cell lysates transfected with either wt N586-Q15 or mtN586-Q68. Four combinations, 2166/HD55, IVLD/2166, IVLD/HD55, and HD55/IVLD, produced strong signals for mu and wt N586; interestingly, there were some reservations about using IVLD and HD55 in combination since both recognize the neoepitope which could have resulted in competition between the two for binding. Nevertheless, due to HD55 being polyclonal and IVLD monoclonal, they appear to work well together. In addition, the signal was shifted further to the right with IVLD/HD55 than IVLD/2166, 2166/HD55, or HD55/IVLD, indicating a slightly higher affinity and thus the best combination. To determine the amount of mtN586, we looked for combinations including MW1 because of its preference for expanded polyglutamine. In our previous screen, MW1 was shown to be a better probe than capture Ab<sup>25</sup>, and the same was seen here, further narrowing the criteria. While both HD55/MW1 and IVLD/MW1 were identified as high affinity combinations, the latter shows the expected preferential recognition of mtN586. Additionally, using IVLD as the capture Ab in both combinations would allow us to

use two separate probes of the same IP, increasing comparative potential. As a result, IVLD/HD55, and IVLD/MW1 were identified as the best highly sensitive pairs with IVLD/HD55 predicted to recognize both wt and mtN586, while IVLD/MW1 is predicted to preferentially recognize mtN586.

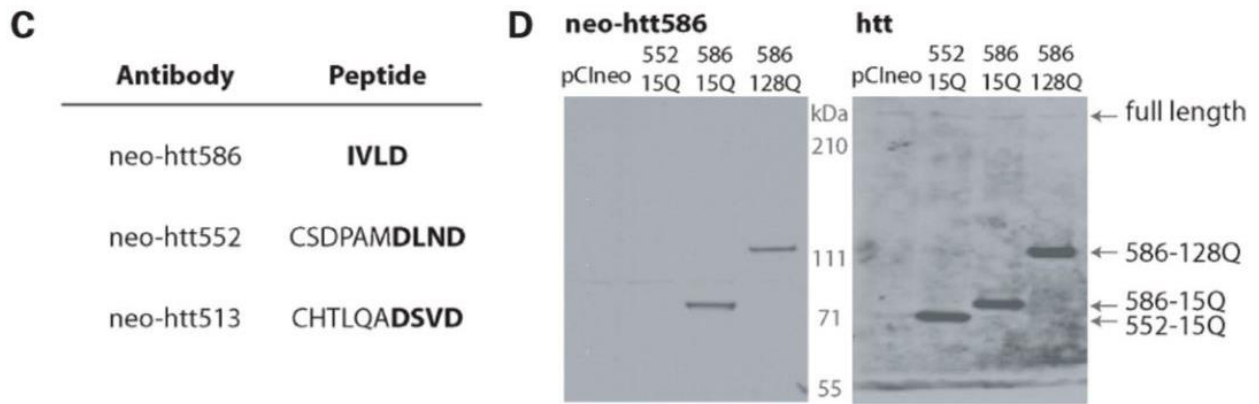


**Figure 3. The neo-htt586 antibody specifically detects huntingtin 586 amino acid fragments.** “(C) Description of the three neo-epitope antibodies used in this study, including the peptides used to generate the antibodies (caspase recognition sequence in bold). (D) By immunoblotting, the neo-htt586 antibody detects the truncated 1-586 amino acid fragments (15 or 28 CAG) but not huntingtin truncated at amino acid 552. As a control, an N-terminal huntingtin antibody (BKP1, right) was used to verify protein expression in extracts from these transfected 293 cells.”<sup>27</sup>

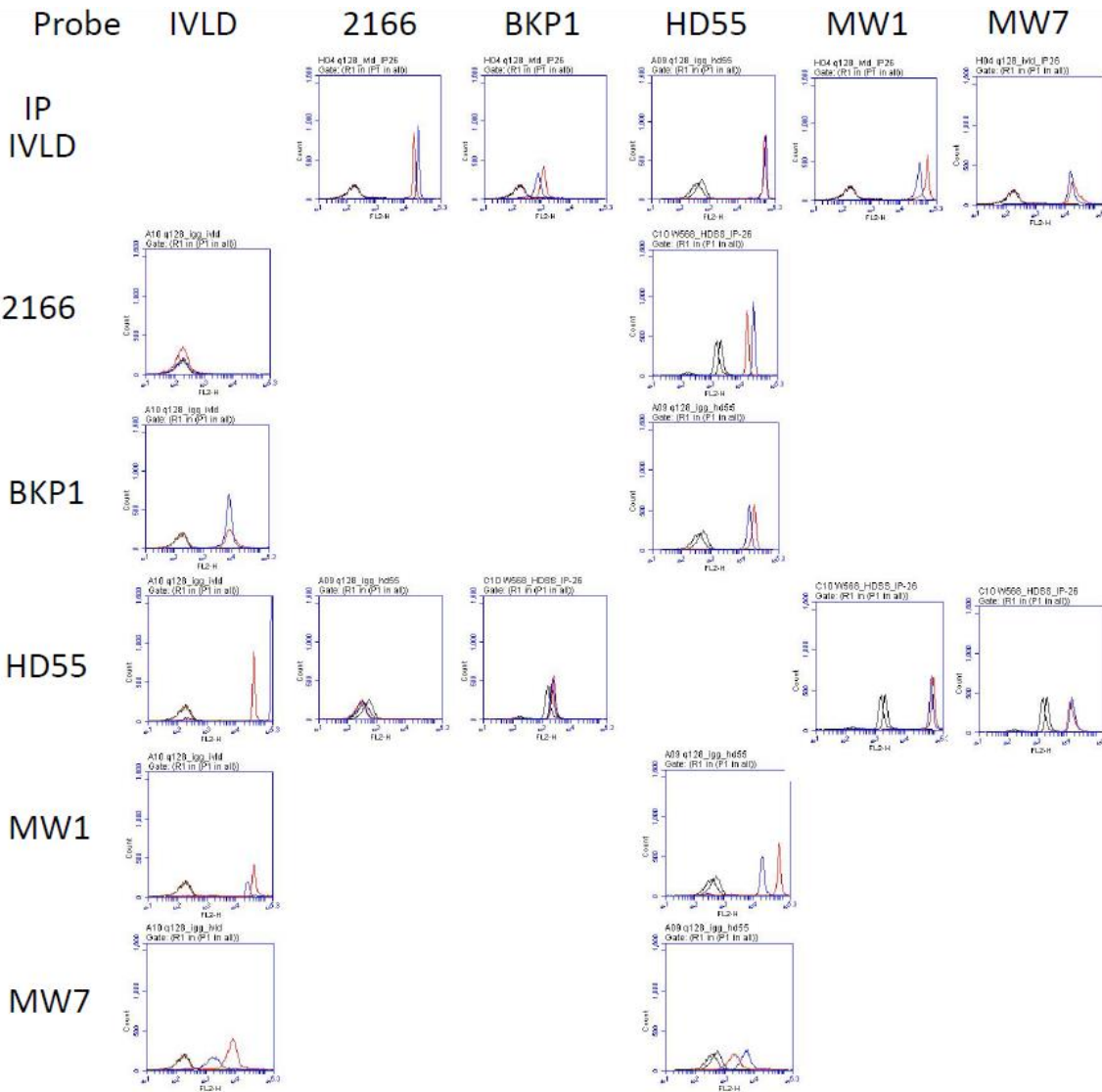


**Figure 4. Screen for N586 IP-FCM capture/probe antibody pairs.** HEK 293 cells were transfected with either wt or mtN586. Cell lysates were used to screen potential N586 IP-FCM capture/probe Ab pairs. Capture Abs are in rows and probe Abs in columns. Median fluorescence intensity vs bead count is graphed. Black traces = beads alone negative control, blue traces = wtN586, red traces = mtN586. Peaks farther to the right of the negative control peak indicate positive detection, with greater magnitude shift indicating higher affinity.

## **Purifying N586 From Brain Lysate Digested With C6 Enzyme**

Characterizing the specificity and sensitivity of the candidate N586 Ab pairs requires purified N586 protein. To generate this, we digested forebrain lysates from Hu97/18<sup>32</sup> humanized HD mice, which contain abundant full-length human wt and mtHTT protein, with purified C6 enzyme. In order to isolate the cut protein of interest, microbeads were activated and bound to IVLD N586-specific Ab. The fragment was then immunoprecipitated with the IVLD coupled beads and eluted with glycine followed by desalting and re-suspension in PBS. Brain lysate, C6 cut lysate, and IVLD immunoprecipitated C6 cut protein were assessed by Western blot to verify the presence of purified N586 after elution from the beads (Figure 5). Comparison of the protein lysate and the C6 cut protein lysate lanes showed an affect from C6 cleavage, as well as an unexpected decrease in the amount of calnexin loading control after C6 digestion, possibly due to cleavage by the enzyme. Further analysis of the immunoprecipitation lane revealed the presence of protein near the predicted size of N586. However, the expected two distinct bands from wt and mtN586 were not observed.

A 10-fold dilution series of the purified protein in artificial CSF (ACSF) was generated to determine the upper and lower limits of assay quantitation. However, N586 IP-FCM with both IVLD/MW1 and IVLD/HD55 failed to produce a reliable signal above assay background (Figure 6), suggesting that either the antibodies weren't recognizing the protein as expected or the protein was not, in fact, N586.



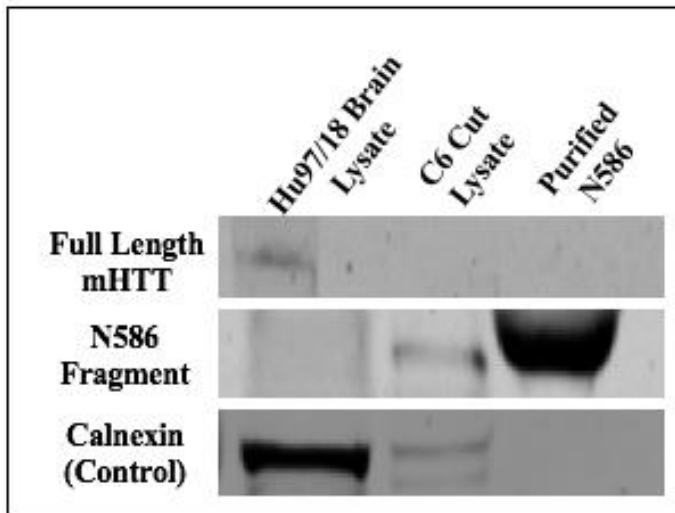


**Figure 5. C6 cut N586 protein Western blot.** Brain tissue lysate from Hu97/18 HD model mice were digested with C6 enzyme to generate N586. Immunoprecipitation with IVLD was used to purify the fragment. Western blotting of brain tissue lysate, C6 cut lysate, and purified N586, with calnexin used as the loading control visualized an effect from C6 cleavage along with an immunoprecipitated protein; however, there weren't two distinct bands for the mt and wtN586 as we had expected.

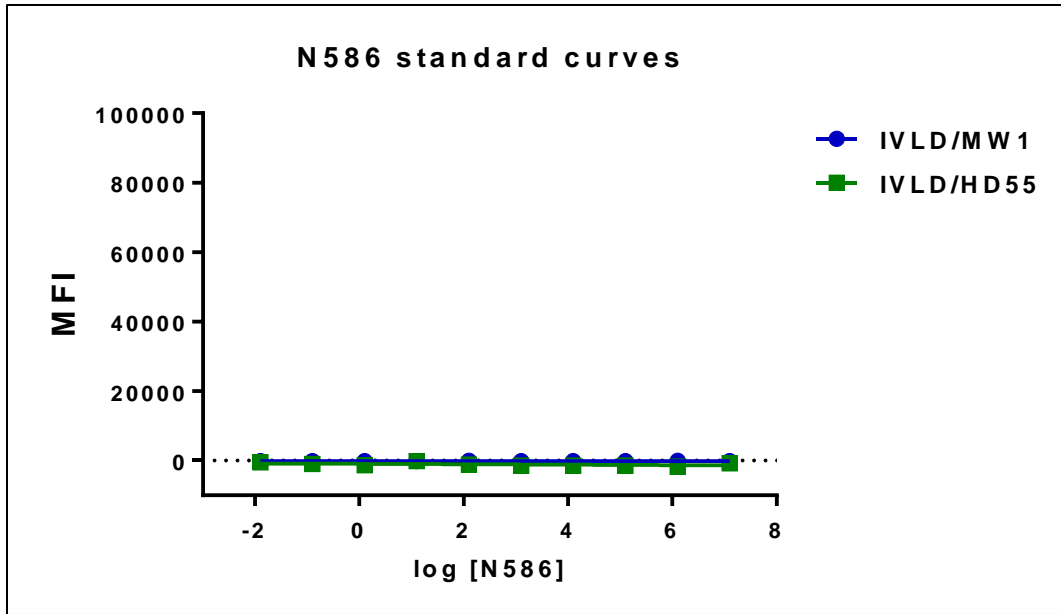


**Figure 6. N586 IP-FCM results with IVLD/MW1 and IVLD/HD55.**

A dilution series of purified N586 was measured with ILVD/MW1 and IVLD/HD55 IP-FCM to characterize assay sensitivity. However, no signal above assay background was detected

## **Purification of Recombinant N586 Protein From Bacterial Expression**

As an alternative approach, we attempted to purify N586 protein produced in bacteria. Bacterial expression constructs used were pMAL-HTT1-586-Q15, expressing wtN586 with 15 glutamine repeats, and pMAL-HTT1-586-Q68, expressing mtN586 with 68 glutamine repeats. The pMAL plasmids express the protein of interest attached to maltose-binding protein (MBP) for isolation of recombinant protein. Plasmids were transformed into BL21(DE3) *E. coli* cells. A restriction enzyme digestion verified the uptake of plasmid into the cells (Figure 7.). Inoculated cultures were grown and induced to produce MBP-N586 with IPTG. After overnight incubation, bacterial cells were lysed and centrifuged and the supernatant containing MBP-N586 was collected. MBP-N586 was isolated from cell lysates through amylose resin column purification, in which the MBP tag binds to the amylose. After washing to ensure flow through of all other cellular contents, MBP-N586 was eluted with free maltose. Eluate was collected in 1ml fractions and measured at A280 to find the fraction with the highest protein concentration (Table 1).

The presence of both N586 fragments were confirmed in this fraction by Western blot. A ponceau stain of the membrane before immunoblotting showed the most prominent protein bands in the samples at ~50 kDa, the expected size of free MBP (Figure 8). We identified N586 fragments at ~ 115 kDa and 121 kDa, representing the smaller wt and larger mtN586 fragments, respectively, after immunoblotting using 2166 anti-HTT Ab (Figure 9), which recognizes an epitope near the C-terminus of N586. However, MW1, which recognizes an epitope near the N-terminus of N586 was unable to recognize MBP-N586 (Figure 9), possibly due to steric hindrance by the N-terminal MBP tag.

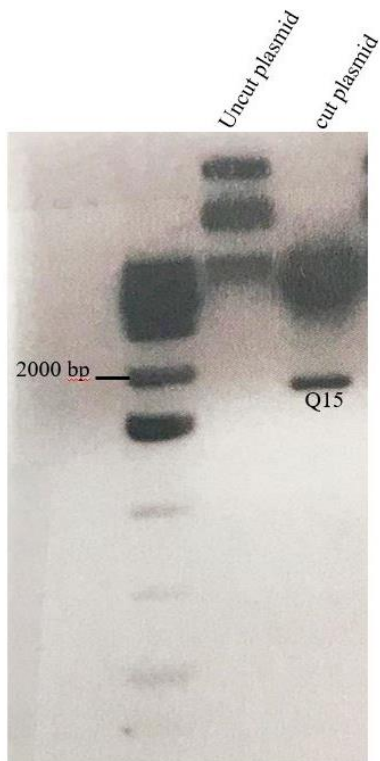


**Figure 7. Restriction enzyme digestion.** Uncut plasmid was digested with NdeI and NotI restriction enzymes and separated by agarose electrophoresis. Uncut plasmid served as the control. A band near the expected molecular weight of Q15 indicated successful transformation had occurred.

**Table 1. Purified N586-Q15 and Q68 MBP fusion protein elution fraction A280 readings**

Sample ID	Date	Conc.	Units	260/280	A280 10mm
Q15_Fraction_1	3/26/18	0.1672	mg/ml	0.84	0.167
<b>Q15_Fraction_2</b>	<b>3/26/18</b>	<b>0.05473</b>	<b>mg/ml</b>	<b>0.56</b>	<b>0.547</b>
Q15_Fraction_3	3/26/18	9.55E-03	mg/ml	0.91	0.01
Q15_Fraction_4	3/26/18	-3.86E-03	mg/ml	1.86	-0.004
Q68_Fraction_1	4/2/18	0.1777	mg/ml	0.75	0.178
<b>Q68_Fraction_2</b>	<b>4/2/18</b>	<b>1.073</b>	<b>mg/ml</b>	<b>0.53</b>	<b>1.073</b>
Q68_Fraction_3	4/2/18	0.0577	mg/ml	0.57	0.058
Q68_Fraction_4	4/2/18	0.01347	mg/ml	0.013	-0.03

**Bolded fractions were retained**

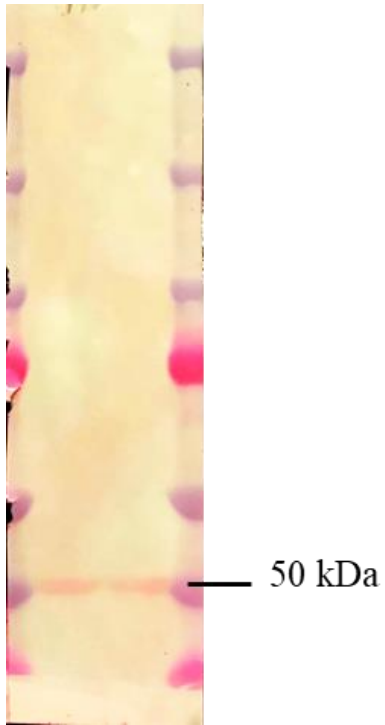


**Figure 8. Ponceau stain of N586.** A ponceau stain of nitrocellulose membrane bound to N586-Q15 and 68 MBP fusion proteins shows a prominent band at the expected size of MBP, ~50 kDa, whereas no bands were apparent at the expected size of MBP-N586-Q15 and Q68.

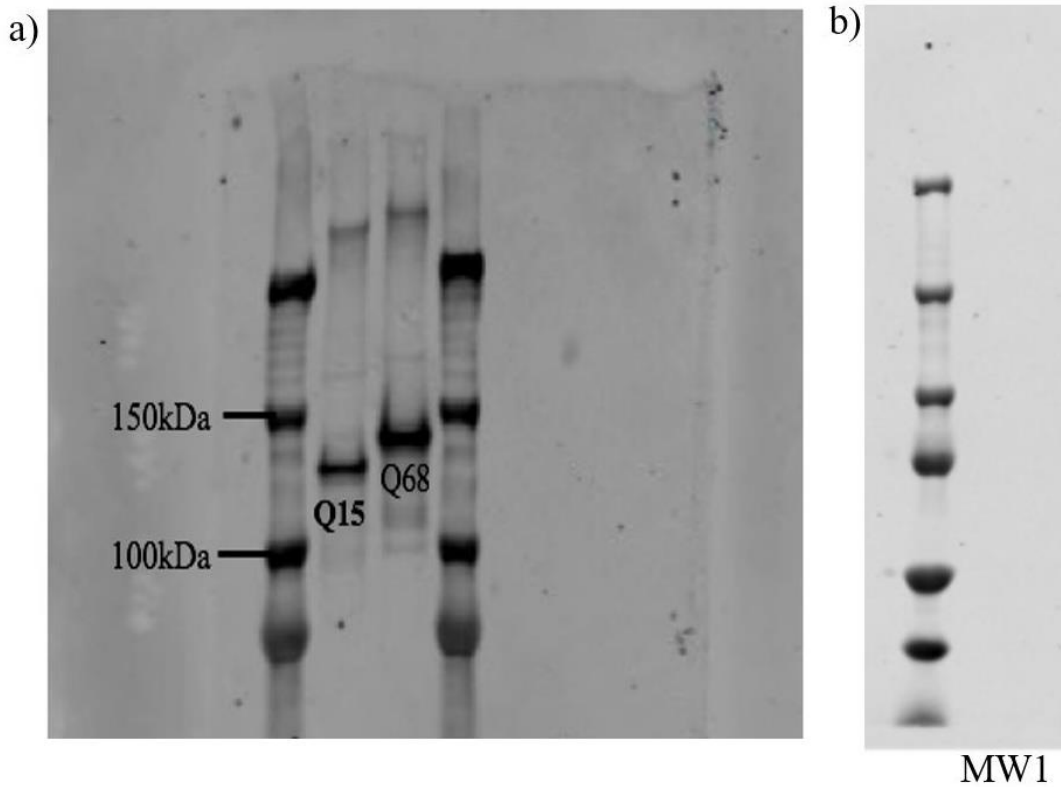


**Figure 9. Recombinant N586 protein Western blot.** Purified N586-Q15 and Q68 recombinant proteins were visualized by Western blot using either primary antibody (A) 2166, which verified the presence of the MBP fusion proteins or (B) MW1, which did not detect the MBP fusion proteins, possibly due to the MBP tag sterically hindering the antibody binding.

### CHAPTER III. DISCUSSION

Due to HTT's inherent size, stickiness, and promiscuity, we encountered technical challenges in generating and purifying recombinant N586. Our first approach for generating purified N586 involved cleavage of exogenously expressed full-length human HTT transgenic proteins in lysates of brain tissue from Hu97/18 humanized HD model mice using purified C6 enzyme, followed by purification of N586 by immunoprecipitation using the neo-epitope specific antibody IVLD. A western blot of the brain lysate, cut lysate, and IP verified that there was an effect of C6 cleavage in the lysate, and a protein was immunoprecipitated; however, the results were not completely as expected, as two distinct bands for the wtHTT with Q18 and mtHTT with Q97 were not visible. In an effort to determine if this was, indeed N586, the purified protein was quantified and a dilution series made in ACSF. IVLD/HD55 and IVLD/MW1 IP-FCM using the purified protein did not detect signal above background, indicating lack of antibody binding either due to a problem with the protein or a problem with the antibody pairs. As these antibody pairs have been previously validated, we opted to use a different method for generation of recombinant N586.

Our second approach involved generation of recombinant N586 using bacterial expression of MBP tagged protein. pMAL-HTT1-586-Q15 and Q68 plasmids were transformed into BL21(DE3) *E. coli*. A restriction enzyme digestion was used to validate successful transformation of plasmid into the cells. Bacterial cultures were then grown to optimum density and induced with IPTG. Amylose resin column purification was used to isolate MBP fusion proteins.



During immunoblotting, a ponceau stain showed a more prominent band at the expected size of free MBP, in comparison to those at the expected sizes of MBP-N586-Q15 and Q68. This suggests that that free MBP is present at greater abundance than N586 in our purified sample. Due to the N-terminal location of the polyQ tract in HTT, only 17 amino acids from the start, HTT expression, particularly with expanded polyQ can be reduced by mRNA quality control processes that reduce translation<sup>33</sup>, which may account for this bias toward free MBP over MBP-N586.

After ponceau staining, the presence of the MBP fusion proteins was verified by Western blot. Due to the proximity of the MW1 epitope to the N-terminal MBP tag, we also wanted to validate binding to the recombinant fusion protein. While we did detect both recombinant proteins showing the expected size shift between the wt and mt forms with the Ab recognizing the C-terminus of N586, we were unable to detect MBP-N586 by Western blot using the anti-polyQ Ab, suggesting that the MBP tag sterically hinders MW1 binding. To overcome this, in ongoing work, we will cleave off the MBP tag and re-purify the protein. HTT is sticky and prone to aggregation, thus untagged recombinant N586 is not expected to remain soluble and available for immunoassay binding once stored. As a result, we will need to complete assay sensitivity characterization immediately upon re-purification. This process will consist of dialysis into PBS to remove free maltose, cleaving off the MBP tag with factor Xa protease, and amylose resin column purification to isolate untagged N586. After cleavage of the MBP tag, we expect normal MW1 binding to the N586 fragment, which we will concurrently verify by Western blot.

Due to the technical challenges in working with untagged N586, we will also try alternative methods for assay specificity characterization. We will digest Hu97/18 and Hu18/18

control littermate primary cortical neuron cell lysates with purified C6 enzyme. While we would be unable to use these lysates for quantitative purposes as the relative amount of N586 in them will not be known, they will allow us to determine qualitatively if an antibody pair recognizes only mtN586 or also wtN586. Additionally, we have contacted Christopher Ross of Johns Hopkins University who has agreed to provide us with flash frozen brain tissue from his transgenic mtN586-82Q mouse line<sup>34</sup>. We will use these tissues to validate assay activity in brain lysate.

If we are able to successfully characterize N586-specific IP-FCM assays, we will use them to look for the presence of N586 in Hu97/18 humanized HD model mouse brain lysate, CSF, and plasma and look for correlations in levels between brain and biofluids. This HD mouse model was chosen for our studies because it expresses only human HTT, so information about immunoassay characteristics will be more translatable as antibody affinity can vary between species. Additionally, human mt and wtHTT are expressed at equivalent levels and total HTT levels are equivalent to normal mouse Htt levels, thus being the closest to endogenous conditions. Whereas if we were to use an overexpression model, we might detect N586 that would not be present in endogenous conditions. If our assays detect N586 in Hu97/18 samples, then we will test HD patient CSF, plasma, and brain tissue lysate to evaluate relevance to human HD. If N586 is detected in patient CSF and/or plasma samples, N586 levels will be correlated to clinical measures to determine if higher or lower levels of N586 are associated with disease.

The results of these studies could be used to identify new therapeutic targets for HD. Rather than targeting C6, which may be deleterious to other biological processes that rely on its enzymatic activity, such as ongoing apoptosis in the colon, selectively targeting the toxic

byproduct of aa586 C6 cleavage would be more direct and likely safer. If we find that N586 persists in tissue and is likely directly toxic, then promoting N586 degradation would be a promising therapeutic strategy. On the other hand, if N586 is rapidly degraded, suggesting that its downstream proteolysis is toxic, stabilizing the N586 fragment may present a more promising therapeutic strategy. All in all, the results of this study could identify new, previously unexplored and more druggable targets for modifying aa586 C6 cleavage-induced toxicity and lead to development of therapies that effectively and selectively inhibit this rate-limiting step in HD pathogenesis.

## CHAPTER IV. METHODOLOGY

### **Primary Antibodies**

MW1 was generated in Paul Patterson's lab<sup>31</sup> and obtained through the Developmental Studies Hybridoma Bank (DSHB) at the University of Iowa. HD55 and IVLD were a gift from the Michael Hayden lab<sup>35</sup>. Additional antibodies were obtained commercially, 2166 (Millipore) and calnexin (Sigma).

### **Hu97/18 Brain Microdissection**

Mice were anesthetized by intraperitoneal injection of 250 mg/kg Avertin and euthanized by cervical dislocation. After decapitation with scissors, the brain was removed and placed on ice for 1 minute to increase tissue rigidity. The hemispheres were partially divided and cortex was peeled back to expose the inner structures. The hippocampus was extracted and placed into a pre-chilled tube, followed by extraction of the striatum and collection of cortex. Brain samples were immediately snap frozen in liquid nitrogen and stored at -80°C until further use.

### **Covalent-Coupling of IVLD to CML Beads**

18x10<sup>6</sup> carboxylate-modified polystyrene latex (CML) beads (5 μm, Interfacial Dynamics Corporation) were washed with 1mL of 2-(N-morpholino)ethanesulfonic acid (MES) buffer (50 mM MES pH 6.0, 1 mM Ethylenediaminetetraacetic acid (EDTA)), and microcentrifuged for 1 minute at 12,000 rpm. The beads were resuspended in 50μL of MES. To activate the beads, fresh 1-Ethyl-3-(3-dimethylaminopropyl)carbodiimide, hydrochloride (EDAC) solution (50mg/mL in MES) was added, and pipetted up and down continuously for 15 minutes. Beads were washed 2-3 times in 1mL of phosphate buffered saline (PBS). IVLD antibody (0.25 mg/mL) was added, and allowed to gently mix for 3-4 hours at room temperature and 1400 rpm on a vortex. Beads were washed 2-3 times with 1mL PBS and resuspended in 100 μl blocking/storage buffer (1% bovine serum albumin (BSA) in PBS + sodium azide (NaN<sub>3</sub>)) to deactivate the beads. A hemocytometer was used to count the beads at a 1:1000 dilution before storage at 4°C until further use.

### **Purification of N586 Protein from Brain lysate**

The right hemisphere of an Hu97/18 humanized HD mouse forebrain was lysed in Nonidet P40 (NP-40) lysis buffer (150 mM sodium chloride (NaCl), 50 mM Tris pH 7.4, Halt Phosphatase and Protease inhibitors (Pierce), 10 mM sodium fluoride (NaF), 10 mM Iodoacetamide, 1% NP40) by homogenization for 10-15s with a mechanical homogenizer followed by incubation on ice for 20 minutes. Lysates were then sonicated for 5 seconds at 25% power and centrifuged at 14,000 rpm at 4°C for 15 minutes to pellet debris. The supernatant was transferred to

microcentrifuge tubes and stored at  $-80^{\circ}\text{C}$  until further use. Protein quantitation was performed with a DC assay kit (Biorad) as per the manufacturer's instructions and absorbance read at 750 nm. A 2-fold dilution series of BSA from 20 mg/ml to 1.25 mg/ml was included to provide a standard curve to obtain the concentration of total protein in the brain lysate.

To cut the HTT protein, 100  $\mu\text{g}$  of brain lysate total protein was digested with 100u/ $\mu\text{l}$  purified C6 enzyme (Enzo Life Sciences Incorporation) in 2X assay buffer (100 mM Hepes, 200 mM NaCl, 0.2% 3-((3-cholamidopropyl) dimethylammonio)-1-propanesulfonate (CHAPs), 2 mM EDTA, 20% glycerol) with 200 mM Dithiothreitol (DTT) and ddH<sub>2</sub>O in a total volume of 70  $\mu\text{l}$  and incubated at  $37^{\circ}\text{C}$  for 1 hour. To immunoprecipitate N586,  $0.5 \times 10^5$  IVLD coupled CML latex beads were added to 50  $\mu\text{l}$  C6 cut lysate and placed on a vertical rotating wheel overnight at  $4^{\circ}\text{C}$ . Beads were washed two times in 1.0 mL of ice-cold IP-FCM buffer (100 mM NaCl, 50 mM Tris pH 7.4, 1% BSA, 0.01% NaN<sub>3</sub>) and centrifuged at 20,000g at  $4^{\circ}\text{C}$  for 3 minutes after each wash. Beads were resuspended in 50  $\mu\text{l}$  PBS. A DC assay was used to quantify the immunoprecipitated protein as described above. To remove the protein from the Ab-coupled beads, the sample was incubated using 3 x 50  $\mu\text{L}$  of glycine (0.2 M, pH 2.6) with frequent agitation for 10 minutes followed by gentle centrifugation at 2000 rpm for 2 minutes and neutralization with an equal volume of Tris pH 8.0. Our protein was buffer exchanged into PBS using a desalting spin column (Zeba) according to the manufacturer's instructions.

## **Western Blotting**

Western blotting was performed to visualize cut and purified protein. Samples containing either 30  $\mu\text{g}$  of brain lysate total protein, 30  $\mu\text{g}$  of C6 cut brain lysate total protein, 4  $\mu\text{g}$  of total IP protein, or 1  $\mu\text{g}$  of total recombinant MBP-N586 protein were combined in a total volume of 25  $\mu\text{l}$  with 4  $\mu\text{l}$  6X Lithium dodecyl sulfate (LDS) loading buffer (Invitrogen), 1  $\mu\text{l}$  1.0 M DTT, and ddH<sub>2</sub>O, and heated at 90°C for 10 minutes to allow denaturation. Proteins were separated by sodium dodecyl sulfate polyacrylamide gel electrophoresis (SDS-PAGE) using a 3-8% Tris acetate Nupage gel (ThermoFisher). Separated proteins were transferred onto a 0.45  $\mu\text{m}$  nitrocellulose membrane. To visualize all transferred proteins, the membrane was stained in 5ml Ponceau S solution (Fisher) and placed on an orbital shaker for 5 minutes at room temperature, then rinsed with ddH<sub>2</sub>O 2-3 times with shaking to remove the background staining.

Immunoblotting was performed using primary antibodies for the C-terminus of the N586 epitope (MAB 2166, 1:2000), expanded polyQ (MW1, 1:500), and calnexin loading control (1:10,000). Secondary antibodies used were IR dye 800CW goat anti-mouse (1:250, Rockland) and AlexaFluor 680 goat anti-rabbit (1:250, Molecular probes). Proteins were visualized using the LiCor Odyssey Imaging System.

## **IP-FCM of Brain Lysate**

A 10-fold dilution series of purified N586 from  $1.26 \times 10^7$  pM to  $1.26 \times 10^{-2}$  pM in a total volume of 50  $\mu\text{L}$  was generated using PBS as diluent. N586 molecular weight was estimated as the mean of the predicted molecular weights of N586-18Q and N586-97Q, considering that the two

proteins should be present at equal proportions in the IP sample. Biotinylation of probe antibodies, HD55 and MW1, was conducted using EZ-Link Sulfo-NHS-Biotin (Thermoscientific), and free biotin was removed with buffer exchange in Amicon Ultra 3K MWCO spin columns (Millipore). The antibody concentration was brought to 0.5 mg/ml and stored at 4°C in PBS. Approximately  $10^4$  IVLD-coupled CML beads in 5  $\mu$ l NP40 buffer were mixed with 50  $\mu$ l of brain lysate and left to immunoprecipitate overnight at 4°C with rotation to prevent beads settling out of suspension. Beads with bound protein were washed in IP-FCM buffer and incubated with biotinylated probe antibodies for 2 hours with rotation, followed by another wash in IP-FCM buffer. The bound complex of bead coupled capture antibody, target protein, and biotinylated probe antibody was then incubated for 1 hour with 1:200 Streptavidin-PE fluorophore (BD Biosciences), followed by a final wash and resuspension in 200  $\mu$ l of IP-FCM buffer. Median fluorescence intensity (MFI) of beads was measured using an Accuri C6 flow cytometer (BD Biosciences) at a speed of 14  $\mu$ l/min until approximately 3000 to 4000 total events were counted. Bead doublets were gated out based on forward scatter area vs. forward scatter height plots, and a singlet bead gate was defined based on forward scatter height vs. side scatter height. All samples were run in duplicate and the average of the MFIs was scored. A reaction containing unconjugated beads alone was used as a negative control, and this blank value was subtracted from all experimental MFIs prior to data analysis. Prism 7 software (GraphPad) was used to generate exponential growth nonlinear fit lines of MFI vs. log [N586].



### **Generation of Recombinant N586 Protein**

BL21 DE3 cells (NEB) were transformed with pMAL-HTT1-586-Q15 or pMAL-HTT1-586-Q68 plasmids according to the supplier's instructions and grown overnight at 37°C on LB-agar plates containing 100 µg/L ampicillin (Amp). Single Colonies were chosen from the plates and used to inoculate 6ml of 2XYT Broth with 100 µg/L Amp, which were grown overnight in a shaking incubator at 37°C and 245 rpm. After 16 hours, plasmid DNA was purified from 3 mL of inoculated culture using a mini-prep kit (Qiagen) according to the manufacturer's instructions. The purified DNA was digested simultaneously with NdeI and NotI restriction enzymes (NEB) to release the N586 insert and separated using a 1.2% agarose-TBE gel to verify insert and vector size. Once the plasmids were validated, the remaining 3 mL of inoculated culture was transferred to 500 mL of fresh 2XYT-Amp Broth and grown until OD 600 value reached 0.6 nm as measured using a nanodrop spectrometer. Plasmid protein expression was then induced by adding 0.5mM IPTG (Thermoscientific) and cultures were incubated at 4°C for 16-24 hours on an orbital shaker. This low temperature was used during N586 expression because it inhibits aggregation of expanded polyQ proteins (Personal communication, Hailey Findlay-Black). Cultures were centrifuged to remove media and the bacterial pellets were stored at -80°C until use.

### **Purification of MBP-tagged Proteins**

Bacterial cell pellets were resuspended in column buffer (Tris-HCl pH 7.4, NaCl, EDTA, and DTT), using approximately 5 mL of buffer per gram of cells, and frozen overnight at -20°C. The

next day, samples were thawed and sonicated three times for 30 seconds at 25% amplitude. Samples were centrifuged at 20,000g for 20 min at 4°C to remove cellular debris and collect the lysates. Protein purification columns were prepared by loading amylose resin slurry (20% ethanol) into 2ml disposable polystyrene columns (Thermofisher) until there was approximately 1 mL of settled beads. The columns were washed twice with 5 volumes of column buffer. Supernatant was loaded into the columns and allowed to flow through completely. The column was washed with buffer until the A280 was negligible, indicating complete flow through of all unbound proteins. Recombinant MBP-N586 proteins were eluted with 5 volumes of 10 mM Maltose elution buffer, collecting 1ml fractions and measuring at A280 to find the fraction with the highest protein concentration.

## REFERENCES

- 1 Group, T. H. D. C. R. A novel gene containing a trinucleotide repeat that is expanded and unstable on Huntington's disease chromosomes. The Huntington's Disease Collaborative Research Group. *Cell* **72**, 971-983 (1993).
- 2 McNeil, S. M. *et al.* Reduced penetrance of the Huntington's disease mutation. *Human Molecular Genetics* **6**, 4 (1997).
- 3 Langbehn, D. R., Hayden, M. R. & Paulsen, J. S. CAG-repeat length and the age of onset in Huntington disease (HD): A review and validation study of statistical approaches. *American Journal of Medical Genetics Part B: Neuropsychiatric Genetics* **153B**, 397-408 (2010).
- 4 Vonsattel, J. P., Keller, C. & Cortes Ramirez, E. P. Huntington's disease - neuropathology. *Handbook of Clinical neurology* **100**, 83-100 (2011).
- 5 Lanciego, J. L., Natasha Luquin, and José A. Obeso. Functional Neuroanatomy of the Basal Ganglia. *Cold Spring Harbor Perspectives in Medicine* **2** (2012).
- 6 Vonsattel, J. P. & DiFiglia, M. Huntington Disease. *J Neuropathol Exp Neurol* **57**, 369-384 (1998).
- 7 Bano, D., Zanetti, F., Mende, Y., & Nicotera, P. . Neurodegenerative processes in Huntington's disease. *Cell Death and Disease* **2** (2011).
- 8 Tabrizi, S. J. *et al.* Predictors of phenotypic progression and disease onset in premanifest and early-stage Huntington's disease in the TRACK-HD study: analysis of 36-month observational data. *The Lancet Neurology* **12**, 637-649 (2013).
- 9 Ross, C. A. & Tabrizi, S. J. Huntington's disease: from molecular pathogenesis to clinical treatment. *The Lancet Neurology* **10**, 83-98 (2011).
- 10 Bates, G. P. *et al.* Huntington disease. *Nature Reviews Disease Primers* **1**, 15005 (2015).
- 11 Samuel, F. Treatment of Huntington's Disease. *Neurotherapeutics* **11**, 7 (2014).
- 12 Zuccato, C., Valenza, M. & Cattaneo, E. Molecular mechanisms and potential therapeutical targets in Huntington's disease. *Physiol. Rev.* **90**, 905-981, doi:10.1152/physrev.00041.2009 (2010).
- 13 Landles, C., and Gillian P. Bates. Huntingtin and the Molecular Pathogenesis of Huntington's Disease. *EMBO Reports* **5**, 20 (2004).
- 14 Shirasaki DI, G. E., Al-Ramahi I, Gray M, Boontheung P, Geschwind DH, Botas J, Coppola G, Horvath S, Loo JA, Yang XW. Network organization of the huntingtin proteomic interactome in mammalian brain. *neuron* **75**, 16 (2012).
- 15 McGarry, A. A randomized, double-blind, placebo-controlled trial of coenzyme Q10 in Huntington Disease. *Neurology* **88**, 7 (2016).
- 16 Hersch, S. M. *et al.* The CREST-E Study of Creatine for Huntington Disease: A Randomized Controlled Trial. *Neurology* **89**, 7 (2017).

- 17 Rodrigues, F. B., and Edward J. Wild. Clinical Trials Corner: September 2017. *Journal of Huntington's Disease* **6**, 8 (2017).
- 18 Leuti, A. *et al.* Phosphodiesterase 10A (PDE10A) localization in the R6/2 mouse model of Huntington's disease. *Neurobiology of Disease* **52**, 12 (2013).
- 19 Van Raamsdonk, J. M. *et al.* Cognitive dysfunction precedes neuropathology and motor abnormalities in the YAC128 mouse model of Huntington's disease. *J Neurosci* **25**, 4169-4180 (2005).
- 20 Slow, E. J. *et al.* Selective striatal neuronal loss in a YAC128 mouse model of Huntington disease. *Hum Mol Genet* **12**, 1555-1567 (2003).
- 21 Godefroy, N., Foveau, B., Albrecht, S., Goodyer, C. G. & LeBlanc, A. C. Expression and activation of caspase-6 in human fetal and adult tissues. *PLOS ONE* **8**, e79313, doi:10.1371/journal.pone.0079313 (2013).
- 22 Qin, Z. & Gu, Z. Huntingtin processing in pathogenesis of Huntington disease. *Acta pharmacologica Sinica (monthly)* **25**, 1243-1249 (2004).
- 23 Pouladi, M. A., Morton, A. J. & Hayden, M. R. Choosing an animal model for the study of Huntington's disease. *Nat Rev Neurosci* **14**, 708-721 (2013).
- 24 Van Raamsdonk, J. M. *et al.* Body weight is modulated by levels of full-length Huntingtin. *Human Molecular Genetics* **15**, 1513-1523, doi:10.1093/hmg/ddl072 (2006).
- 25 Southwell, A. L. *et al.* Ultrasensitive measurement of huntingtin protein in cerebrospinal fluid demonstrates increase with Huntington disease stage and decrease following brain huntingtin suppression. *Scientific Reports* **5**, 12166 (2015).
- 26 Schrum, A. G. *et al.* High-sensitivity detection and quantitative analysis of native protein-protein interactions and multiprotein complexes by flow cytometry. *Science Signaling* **2007**, pl2-pl2, doi:10.1126/stke.3892007pl2 (2007).
- 27 Warby, S. C. *et al.* Activated caspase-6 and caspase-6-cleaved fragments of huntingtin specifically colocalize in the nucleus. *Human Molecular Genetics* **17**, 2390-2404, doi:10.1093/hmg/ddn139 (2008).
- 28 Southwell, A. L. *HD Insights: A Huntington disease research periodical* **12** (2015).
- 29 Wellington, C. L. *et al.* Caspase cleavage of mutant huntingtin precedes neurodegeneration in Huntington's disease. *The Journal of Neuroscience* **22**, 7862-7872 (2002).
- 30 Cong SY, Pepers BA, Roos RA, Van Ommen GJ & JC., D. Epitope mapping of monoclonal antibody 4C8 recognizing the protein huntingtin. *Hybridoma* **24** (2005).
- 31 Ko, J., Ou, S. & Patterson, P. H. New anti-huntingtin monoclonal antibodies: implications for huntingtin conformation and its binding proteins. *Brain Res Bull* **56**, 319-329 (2001).
- 32 Southwell, A. L. *et al.* A fully humanized transgenic mouse model of Huntington disease. *Human Molecular Genetics* **22**, 18-34, doi:10.1093/hmg/dds397 (2013).
- 33 Richards, J., Sundermeier, T., Svetlanov, A. & Karzai, A. Quality control of bacterial mRNA decoding and decay. *Biochemica et biophysica acta* **1779**, 8 (2008).

- 34 Waldron-Roby, E. *et al.* Transgenic mouse model expressing the caspase 6 fragment of mutant huntingtin. *Journal of Neuroscience* **32**, 10, doi:10.1523/JNEUROSCI.1305-11.2012 (2012).
- 35 Warby, S. C. *et al.* Activated caspase-6 and caspase-6-cleaved fragments of huntingtin specifically colocalize in the nucleus *Human Molecular Genetics* **17**, 14 (2008).